RSC Advances

ROYAL SOCIETY OF CHEMISTRY

www.rsc.org/advances

Water-catalysis in the Gas Phase Reaction of Dithioformic Acid with Hydroxyl Radical: Global Reaction Route Mapping of Oxidative Pathways for Hydrogen abstraction

Gurpreet Kaur and Vikas*

Quantum Chemistry Group, Department of Chemistry & Centre of Advanced Studies in Chemistry, Panjab University, Chandigarh- 160014 INDIA.

*Corresponding Author

Email: qlabspu@pu.ac.in, qlabspu@yahoo.com

Phone: +91-172-2534408, +91-9855712099

Abstract

The catalytic-role of water in the gas phase oxidation reaction of hydroxyl radical with dithioformic acid (DTFA) has been investigated through quantum mechanical computations performed using MP2, CCSD(T) and DFT methods. The pre-reaction complexes, which can considerably influence the thermodynamics and kinetics, are systematically explored through a global reaction route mapping (GRRM) method. The computations successfully revealed a positive catalytic role of water which is observed to stabilize the pre-reaction complexes as well as respective transition states, resulting in a significant lowering of the potential energy surface. The standard Gibbs free energy change for the explored pathways was also analyzed. The abstraction of acidic-hydrogen in DTFA was found to be both thermodynamically and kinetically more feasible than the formyl-hydrogen abstraction both in the presence and absence of water. Notably, a few of the pathways are observed to proceed through a proton-coupled electron-transfer mechanism. However, only formyl-hydrogen abstraction in the presence of water could be traced by all the different theoretical methods employed in this work.

Keywords: Water catalysis, oxidation, hydrogen abstraction, hydroxyl radical, dithioformic acid, GRRM.

Introduction

In the earth's atmosphere, hydroxyl (OH) radical is known to interact with the polar molecules predominantly in the presence of water with the latter acting as a catalyst.[1-3] The presence of water significantly lowers the potential energy surface (PES) of the reaction by forming the pre-reaction complexes and stabilizing the reaction intermediates through hydrogen bonding [1,4]. We had recently[4] revealed water catalysis in the reaction of hydroxyl radical with thioformic acid (TFA). It was found that the water-catalyzed hydrogen abstraction in TFA was thermodynamically as well as kinetically more favorable than the noncatalytic hydrogen abstraction. The same behavior of water was also observed in our recent work[5] on the exploration of pathways for isomerisation and water migration in the complexes of TFA with single-water molecule. In all these studies, the reaction pathways were traced using a global reaction route mapping (GRRM) method.[3,6-11] The GRRM uses an anharmonic downward distortion following (ADDF) approach for exploring the equilibrium structures (EQs), transition states (TSs) and dissociation channels (DCs) on a PES. It is an uphill walking method compared to the widely used downhill walking methods like intrinsic reaction coordinates (IRC).[12,13] We had successfully employed the GRRM for revealing stereoinversion[14,15] and isomerisation pathways in molecules.[16,17]

However, the actual kinetics and dynamics along a reaction pathway cannot be determined simply through the exploration of various species on a PES. In order to obtain insight at the atomic level, molecular dynamics simulations are necessary.[18-25] In fact, it has been observed that the actual dynamics may overlook a potential energy minimum for a reaction intermediate, even if no barrier is present to access the intermediate.[20,23-24] The atomic-level dynamics may be even more complex for chemical reactions involving solvation by water molecules[25], as also in the case of water-catalyzed reaction which involves at least a three-body system.

The present work investigates the reaction of OH radical with the dithioformic acid (DTFA) to explore probable water-catalytic pathways for the hydrogen abstraction in DTFA. The dithio-carboxylic acids have remained an area of keen research owing to their biochemical applications.[26-28] The compounds containing -S-C(=S) groups are important intermediates in biological processes.[26-28] Moreover, DTFA is an appropriate model to study the conformational changes and its effect in biological molecules.[26-28] For example, it can be used to estimate the structural and dynamical features of dithio acyl enzyme intermediates produced during papain-catalyzed hydrolysis.[26-28] The present work explores water catalysis in the reaction of OH radical with DTFA by exploring the PES as described in the next section, however, no molecular dynamics simulations have been performed in the present work.

Computational methodology

The pre-reaction complexes involving OH radical, DTFA and water, were explored employing a large-ADD-following approach in the GRRM method at the DFT/BHandHLYP/6-311++G(d,p) level of the theory using Becke-half-and-half-Lee-Yang-Parr (BHandHLYP)[29] exchange-correlation (XC) functional of the density functional theory (DFT). In order to search only the lower regions of the PES, five largest ADDs were searched around 20 random structures. The binary complexes, HSCSH-H_2O, depicted in Figures 1-4 for various reaction pathways of DTFA were optimized by removing OH from ternary pre-reaction complexes. All the transition state (TS) structures were obtained by guess and applying the saddle point optimization through the GRRM method. The harmonic vibrational frequency analysis was further performed to test if the optimized geometry obtained is a minimum or a transition state, and to obtain the zero-point energy (ZPE) correction. In order to check the right connectivity between the reactants and products, and to obtain the product

structures, the IRC computations were performed on all the transition states obtained. The energies were refined at the single-point CCSD(T)/6-311++G(d,p) level of the coupled cluster theory,[30] using geometries optimized at DFT/BHandHLYP/6-311++G(d,p) level of theory, which were further corrected for the basis set superposition error (BSSE) employing counterpoise method.[31]

For comparison, the geometries of the pre-reaction complexes and TSs obtained at the level of DFT/BHandHLYP/6-311++G(d,p) are further optimized employing Møller-Plesset perturbation theory[32] at MP2/6-311++G(2d,2p) level, and single-point energies were also computed at the CCSD(T)/6-311++G(2d,2p)//MP2/6-311++G(2d,2p) level. Further, in order to confirm the reaction pathways traced at the level of DFT/BHandHLYP/6-311++G(d,p), all the transition states were optimized and IRC computations were carried using DFT methods employing a hybrid B3LYP,[33] and a dispersion corrected ω-B97XD[34]XC functionals with basis set 6-311++G(d,p). In order to further account for the self-interaction error (SIE) in the DFT methods, the computations are also carried using M06-HF XC functional which is known to eliminate SIE at long range.[35] Further, to test the dependability of these computations with respect to a multireference character of the wavefunction at the stationary points, T1 diagnostics[36] of the pre-reaction complexes and products were performed at the CCSD/6-311++G(d,p)//DFT/BHandHLYP/6-311++G(d,p) level of the theory. These values were also compared at CCSD/6-311++G(2d,2p)//MP2/6-311++G(2d,2p) levels for pre-reaction complexes only. As evident in Table 1, the T1 diagnostic values were found to be in the range of 0.012 to 0.031, with values for most of the species to be <0.02, marking the reliability of a single-reference methods like CCSD(T) used for the present computations. In the present work, all the required computations for the GRRM program are performed along with the GAUSSIAN 03[37] and 09[38] quantum chemistry software.

Result and Discussions

The trans-conformer of DTFA is found to be 1.32 kcal/mol more stable than cis conformer at CCSD(T)/6-311++G(d,p)//BHandHLYP/6-311++G(d,p) level as has also been observed to be stable by 1.99 kcal/mol in a previous[39] study at MP2/6-31G(d) level of the theory. Following this, our present work focuses on the hydrogen abstraction reactions of only trans-DTFA with OH radical. These reactions can either involve abstraction of the formyl hydrogen (C−H) or the acidic hydrogen (S−H). Various oxidative reaction pathways identified for the formyl and acidic hydrogen abstraction in DTFA are shown in Figures 1 and 2, respectively, in the absence and presence of single-water molecule. The relative potential energy profile of the hydrogen-abstraction pathways explored for the DTFA, at CCSD(T)/6-311++G(d,p)//BHandHLYP/6-311++G(d,p) and other levels of theory employed in the present work, is provided in Figure 3, while the relative energies computed with respect to the sum of separated reactants and T1 diagnostic values of various reaction species are summarized in Table 1. Besides these, the standard Gibbs free-energy change (ΔG) along the pathways is also provided in Table 2, while Table 4 depicts the ΔG relative to the isolated species at different temperatures for the dissociation reaction of binary and ternary complexes into the DTFA, OH and/or water. Since the hydrogen-abstraction in molecules like DTFA is known to proceed via free-radical and proton-coupled electron transfer (PCET)[40]mechanisms, therefore, to further obtain insights into the mechanism of hydrogen-abstraction, spin density distribution, obtained from the natural bond orbital (NBO)[41] analysis, on atoms in molecular species explored along the pathways is provided in Table 3. Besides this, the molecular orbitals (MOs) of transition states are also analysed which are further depicted in Figure 4.

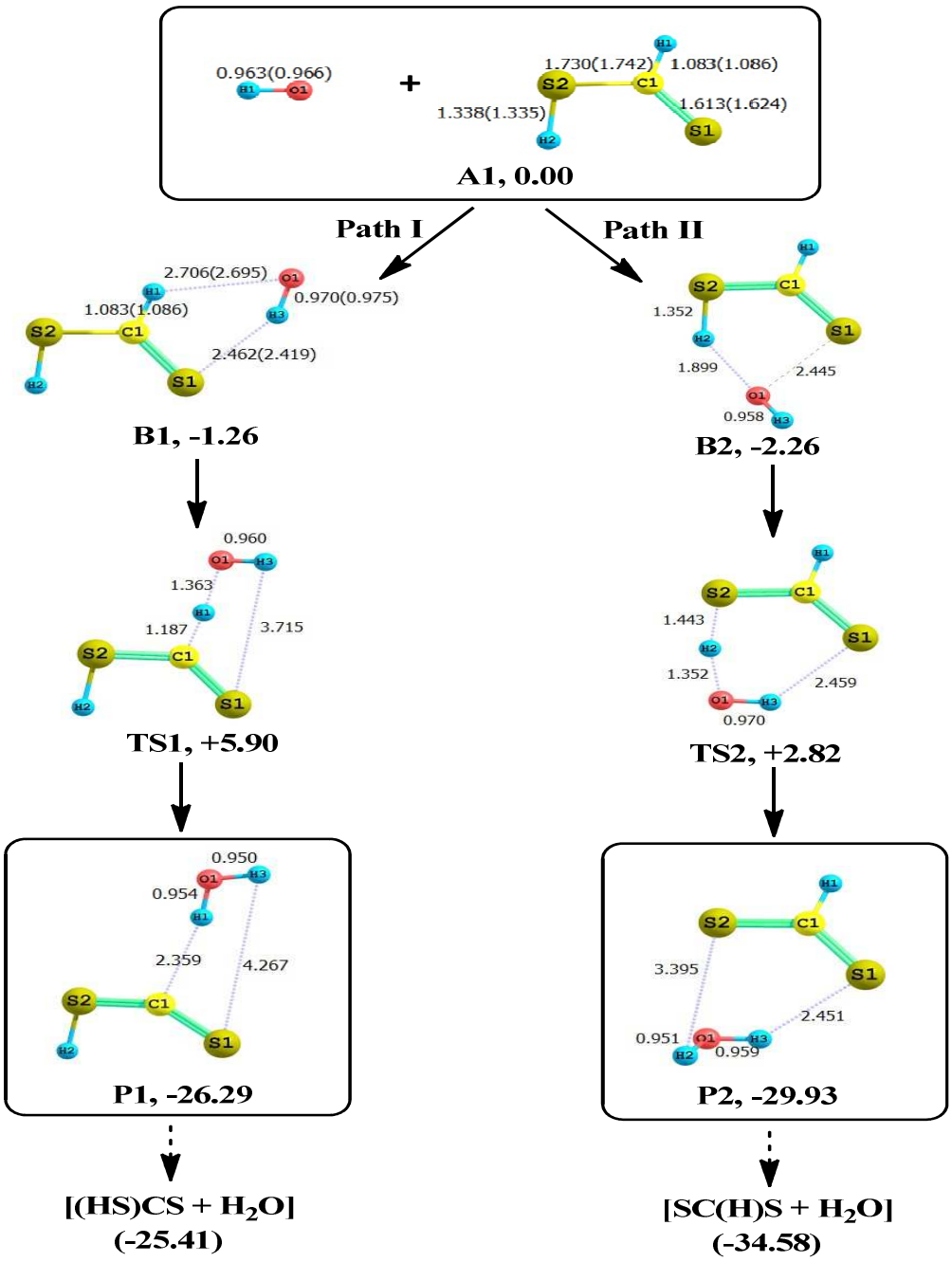

Figure 1. Oxidation pathways I and II, respectively, for the noncatalytic formyl and acidic hydrogen abstraction of DTFA. The numerical values depicted in bold are relative energies (in kcal/mol) with respect to isolated reactants A1, are computed at the CCSD(T)/6-311++G(d,p)//BHandHLYP/6-311++G(d,p) level including ZPE and BSSE correction. The distances (in Å), depicted with and without parentheses, were optimized at the MP2/6-311++G(2d,2p) and BHandHLYP/6-311++G(d,p) levels, respectively.

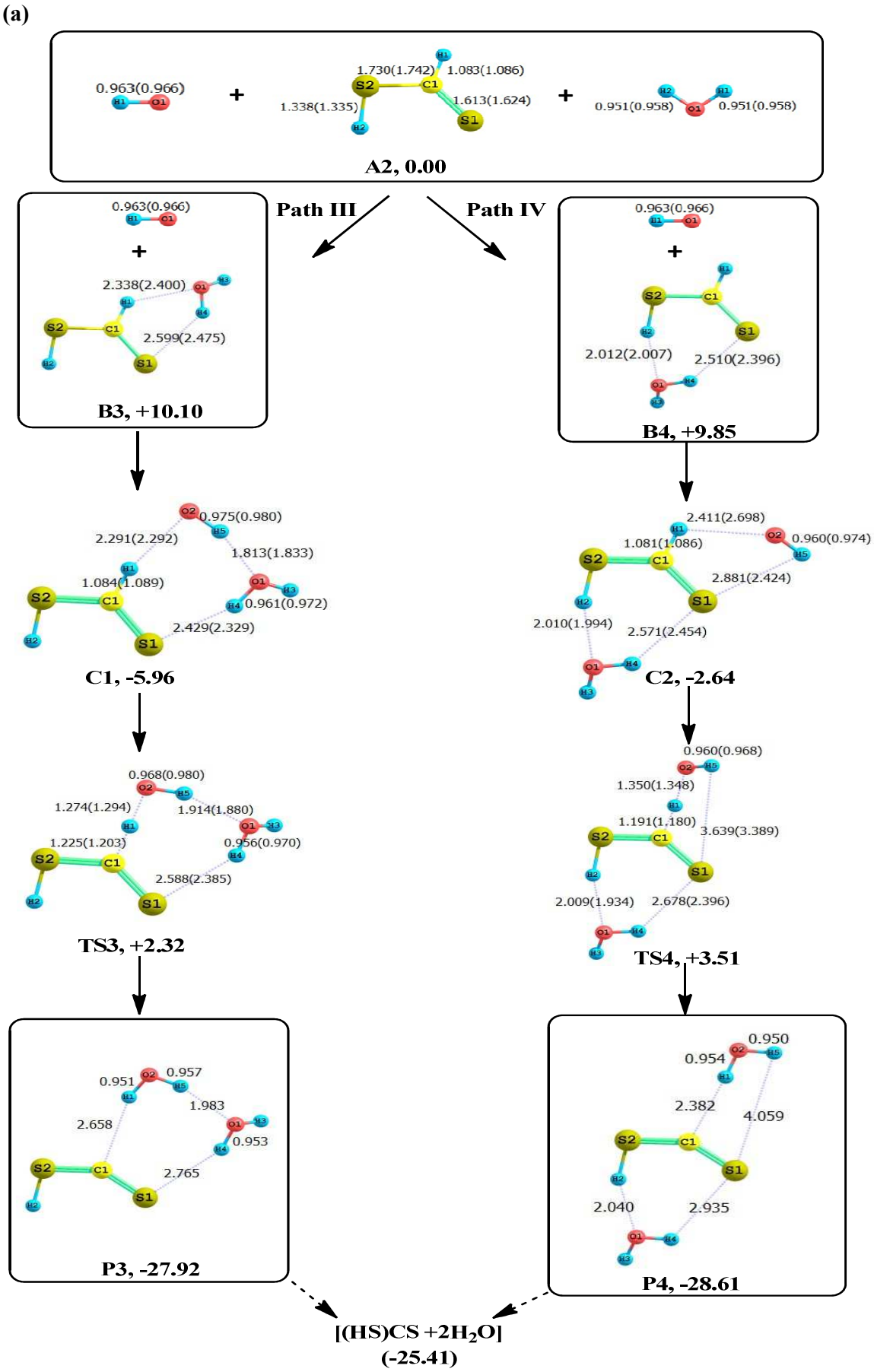

Figure 2.....continued

(b)

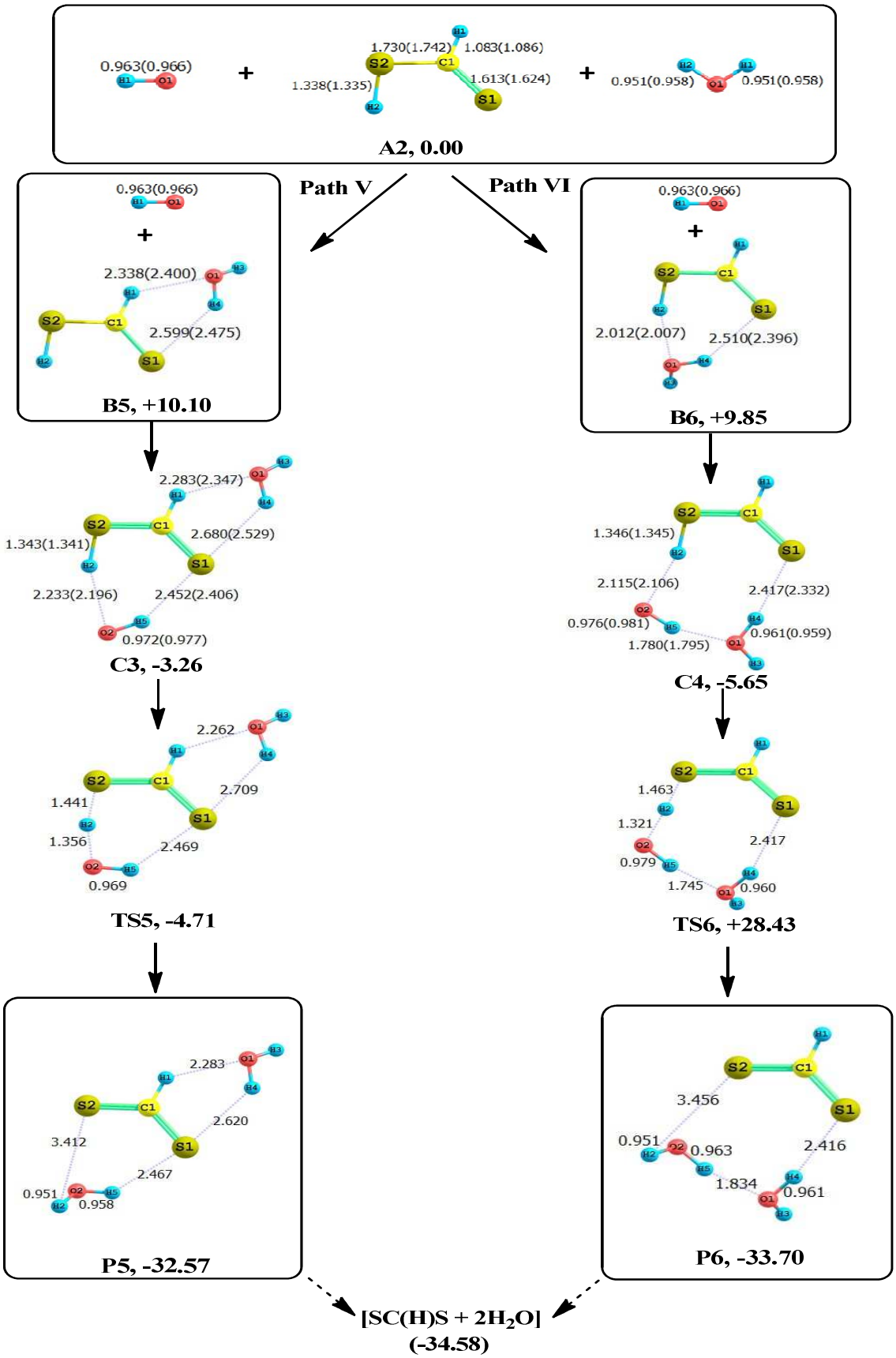

Figure 2……continued

(c)

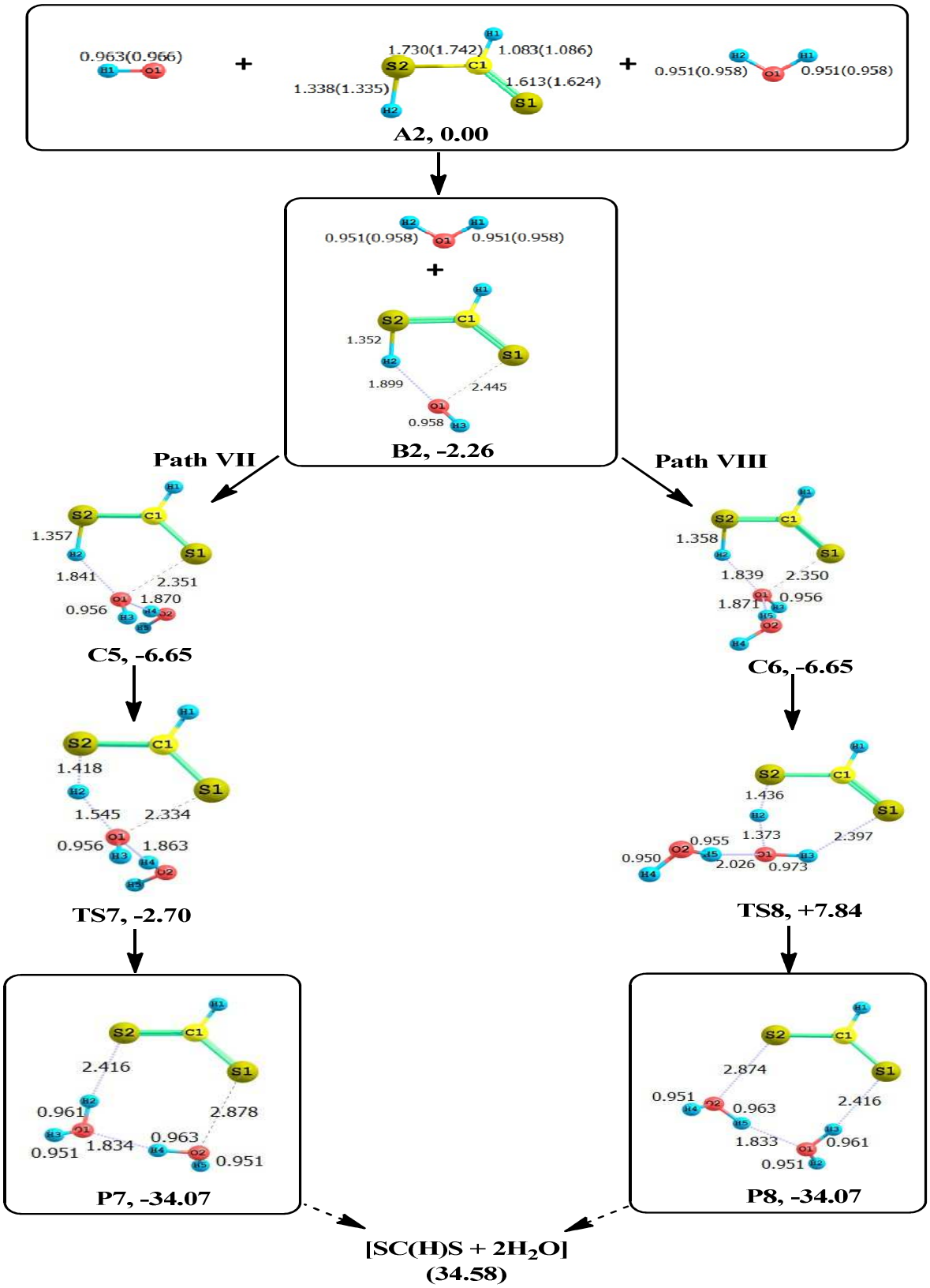

Figure 2. Same as Figure 1 but for the oxidation pathways involving water-catalyzed (a) formyl, (b) and (c) acidic hydrogen abstraction of DTFA. The relative energies, including ZPE and BSSE correction, depicted in bold are with respect to isolated reactants A2.

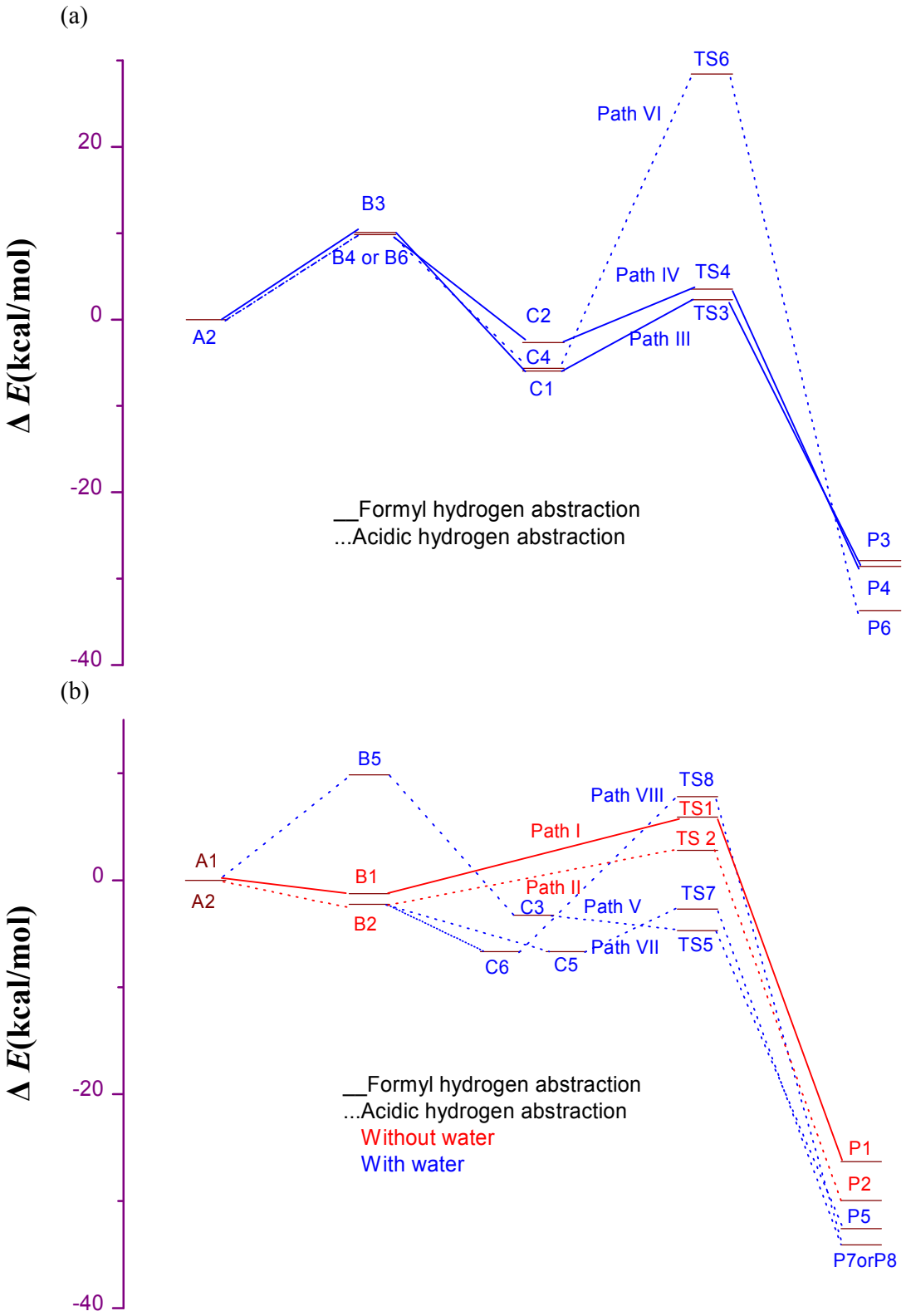

Figure 3. Relative energy profile (in kcal/mol), including ZPE and BSSE correction, for various oxidative reaction pathways depicted in Figures 1 and 2, at the CCSD(T)/6-311++G(d,p)//BHandHLYP/6-311++G(d,p) level of the theory, (a) pathways traced by all the theoretical methods employed, except Path VI which was detected only using DFT methods employing BHandHLYP, B3LYP, ω-B97XD and M06-HF functionals, (b) additional pathways traced using the DFT/BHandHLYP method. Path II was also traced through the DFT/M06-HF method.

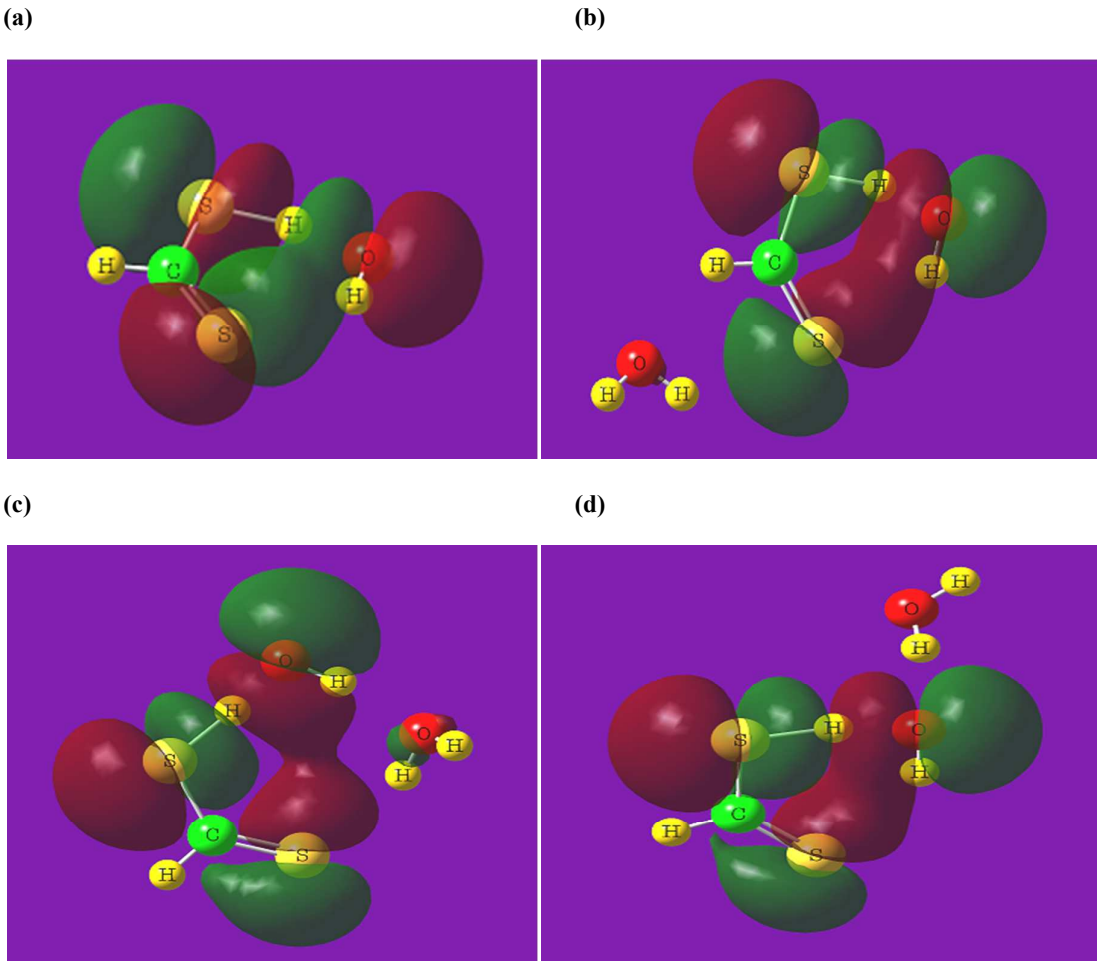

Figure 4. 3D surface plots (isovalue=0.02) of singly occupied β molecular orbitals (MOs) depicting a probable PCET in the transition states (a) TS2 (b) TS5 (c) TS6 (d) TS8 at DFT/UBHandHLYP/6-311++G(d,p) level of the theory. For TS2, TS6 and TS8 the plots correspond to highest occupied β MOs.

Table 1. Relative energy (in kcal/mol) of stationary points (depicted in Figures 1-3) with respect to the separated reactants at ZPE and BSSE corrected CCSD(T)/6-311++G(d,p)//BHandHLYP/6-311++G(d,p), and CCSD(T)/6-311++G(2d,2p)//MP2/6-311++G(2d,2p) levels of the theory. The BSSE correction for the transition states energy is computed taking hydrogen being abstracted as fragment. T1 diagnostics are listed for ternary pre-reaction complexes, at CCSD/6-311++G(d,p)//DFT/BHandHLYP/6-311++G(d,p) and CCSD/6-311++G(2d,2p)//MP2/6-311++G(2d,2p) levels (indicated in parenthesis).

Stationary points	BHandHLYP /6-311++G(d,p) + ZPE[a] +BSSE	BSSE at BHandHLYP /6-311++G (d,p)	MP2/6-311++G(2d, 2p) +ZPE[b] +BSSE	BSSE at MP2/6-311++G(2 d,2p)	CCSD(T)/6-311++G(d,p) // BHandHLYP /6-311++G(d,p) + ZPE[a] +BSSE	BSSE at CCSD(T)/6-311++G(d,p) // BHandHLYP /6-311++G(d,p)	CCSD(T)/6-311++G(2d,2p) // MP2/6-311++G(2d,2p) +ZPE[b] +BSSE	BSSE at CCSD(T)/ 6-311++G(2 d,2p) // MP2/ 6-311++G(2 d,2p)	T1 diagnostic
B1[c]	-1.63	0.38	+66.14	1.07	-1.26	1.82	-5.21	1.26	0.017(0.017)
TS1*[c]	+4.20	1.69			+5.90	6.84			
P1[c]	-22.15	0.63			-26.29	1.76			0.016
B2*[c]	-3.89	0.69			-2.26	4.20			0.031
TS2*[c]	+0.38	1.00			+2.82	6.90			
P2[c]	-29.56	0.44			-29.93	3.14			0.019
B3	-2.82	0.31	-2.51	1.13	+10.10	1.88	+10.79	1.32	
C1[c]	-7.59	0.94	-4.77	2.57	-5.96	4.46	-4.46	3.07	0.013(0.012)
TS3[c]	-0.50	2.57	+6.15	5.96	+2.32	9.91	+1.57	7.22	
P3[c]	-24.66	1.32			-27.92	3.89			0.016
B4	-4.02	0.56	-3.33	1.57	+9.85	2.70	+10.23	1.88	
C2[c]	-6.40	0.82	-5.71	2.57	-2.64	4.96	-5.15	3.07	0.019(0.013)
TS4[c]	+0.44	2.38	+7.03	5.77	+3.51	9.29	+2.56	7.03	
P4[c]	-25.67	1.19			-28.61	3.89			0.015
B5	-2.82	0.31	-2.51	1.13	+10.10	1.88	+10.79	1.32	
C3[c]	-4.77	0.56	-4.89	2.38	-3.26	3.70	-4.71	2.82	0.013(0.013)
TS5*[c]	-2.64	1.44			-4.71	8.53			
P5[c]	-31.50	2.13			-32.57	4.77			0.015
B6	-4.02	0.56	-3.33	1.57	+9.85	2.70	+10.23	1.88	
C4[c]	-7.22	1.00	-4.39	2.76	-5.65	4.52	-3.95	3.26	0.013(0.013)
TS6*[c]	-3.51	1.88			+28.43	9.73			
P6[c]	-33.20	2.82			-33.70	5.71			0.017
B2*[c]	-3.89	0.69			-2.26	4.20			
C5*[c]	-8.09	1.32			-6.65	7.15			0.030
TS7*[c]	-8.22	1.76			-2.70	13.11			
P7[c]	-33.13	2.82			-34.07	5.33			0.017
B2*[c]	-3.89	0.69			-2.26	4.20			
C6*[c]	-8.09	1.32			-6.65	7.15			0.030
TS8*[c]	-1.32	1.32			+7.84	8.41			
P8[c]	-33.13	2.82			-34.07	5.33			0.017

*corresponds to species which failed to optimize at theMP2/6-311++G(2d,2p) level of the theory. [c]complexes are computed at default unrestricted levels of theory.

Table 2. Standard Gibbs free energy change (ΔG) in kcal/mol, at BHandHLYP/6-311++G(d,p) and CCSD(T)/ 6-311++G(d,p)// BHandHLYP/6-311++G(d,p) levels, for the reaction pathways depicted in Figures 1 and 2.

Reaction Pathways		BHandHLYP/6-311++G(d,p)	CCSD(T)/ 6-311++G(d,p)// BHandHLYP/6-311++G(d,p)
Path I	B1→TS1	6.34	7.66
	TS1→P1	-28.61	-34.45
Path II	B2→TS2	4.52	5.33
	TS2→P2	-30.94	-33.76
Path III	C1→TS3	8.09	9.29
	TS3→P3	-27.80	-33.70
Path IV	C2→TS4	7.22	6.53
	TS4→P4	-29.24	-35.08
Path V	C3→TS5	3.01	-0.56
	TS5→P5	-29.81	-28.61
Path VI	C4→TS6	5.02	35.39
	TS6→P6	-31.25	-63.50
Path VII	C5→TS7	0.56	4.64
	TS7→P7	-25.85	-32.13
Path VIII	C6→TS8	6.15	13.87
	TS8→P8	-31.44	-41.35

Table 3. Spin density distribution determined from NBO analysis of pre-reaction complexes and transition states involved in the hydrogen abstraction reaction of DTFA with OH with and without water at BHandHLYP/6-311++G(d,p) level of theory.

Species	C1	H1	S1	H2	S2	O1	H3	H4	O2	H5
B1	-0.008	-0.001	0.011	0.000	-0.002	1.024	-0.025			
TS1	**0.198**	**-0.057**	0.171	0.015	0.009	**0.683**	-0.018			
B2	-0.045	0.011	0.340	0.000	-0.002	0.715	-0.020			
TS2	-0.038	0.048	**0.840**	-0.005	0.001	**0.168**	-0.013			
C1	-0.004	-0.005	0.017	0.001	-0.003	-0.001	0.000	0.000	1.017	-0.023
TS3	**0.273**	**-0.071**	0.137	0.021	0.005	0.001	0.000	0.000	**0.649**	-0.015
C2	-0.032	0.005	0.151	0.000	-0.009	0.002	0.000	0.000	0.904	-0.023
TS4	**0.215**	**-0.058**	0.159	0.015	0.005	0.002	0.001	0.001	**0.679**	-0.018
C3	-0.011	0.001	0.015	-0.010	0.016	0.000	0.000	0.000	1.012	-0.024
TS5	-0.045	0.047	**0.796**	0.000	0.024	0.006	0.000	-0.002	**0.188**	-0.012
C4	-0.014	0.002	0.018	-0.011	0.018	0.000	0.000	0.000	1.010	-0.022
TS6	-0.039	0.056	**0.827**	-0.005	0.036	0.011	0.000	-0.004	**0.117**	0.001
C5	-0.056	0.015	0.497	0.001	-0.002	0.562	-0.017	-0.001	-0.001	0.000
TS7	-0.057	0.017	**0.629**	-0.001	-0.008	**0.434**	-0.013	0.000	-0.001	0.000
C6	-0.056	0.015	0.498	0.001	-0.002	0.561	-0.017	0.000	-0.001	-0.001
TS8	-0.053	0.048	**0.869**	-0.002	0.021	**0.131**	-0.015	0.000	0.001	0.000

Table 4. Standard Gibbs free energy change (ΔG) in kcal/mol for the dissociation of binary and ternary pre-reaction complexes, at various temperatures using computations performed at BHandHLYP/6-311++G(d,p) level.

Species	Temperature (in K)						
	100	150	200	250	273.15	298.15	350
Complexes of DTFA with OH radical: DTFA···OH→ DTFA + ·OH							
B1	0.00	-1.26	-2.51	-3.77	-4.33	-5.02	-6.21
B2	2.26	0.75	-0.75	-2.32	-3.01	-3.83	-5.40
Complexes of DTFA with H_2O: DTFA···(H_2O)→ DTFA + H_2O							
B3	0.94	-0.38	-1.69	-2.95	-3.51	-4.14	-5.40
B4	2.32	0.88	-0.63	-2.07	-2.70	-3.45	-4.83
Complexes of DTFA with H_2O and OH radical: DTFA···(OH)···(H_2O)→ DTFA+ ·OH + H_2O							
C1	4.52	1.95	-0.69	-3.33	-4.46	-5.77	-8.35
C2	2.70	-0.06	-2.76	-5.46	-6.71	-8.03	-10.67
C3	1.07	-1.57	-4.20	-6.84	-8.03	-9.29	-11.86
C4	4.08	1.32	-1.51	-4.39	-5.71	-7.15	-9.98
C5	4.96	2.20	-0.63	-3.45	-4.71	-6.15	-8.91
C6	4.96	2.20	-0.63	-3.45	-4.71	-6.15	-8.91

Table 5. Self interaction error (SIE) is computed by comparing ZPE corrected energies at BHandHLYP/6-311++G(d,p) and M06-HF/6-311++G(d,p) levels of theory with respect to energies of the pre-reaction complexes.

Species	BHandHLYP/6-311++G(d,p)	M06-HF/6-311++G(d,p)	SIE
Pathway III			
C1	0	0	0
TS3	+5.9	-1.13	7.03
P3	-17.07	-25.92	8.85
Pathway IV			
C2	0	0	0
TS4	+5.52	+5.71	-0.19
P4	-19.27	-20.96	1.69

Oxidation Pathways

In the water-free environment, two pathways were explored for the oxidation reaction of DTFA with OH radical as depicted in Figure 1. Pathway I involve formyl H-abstraction which results into single water molecule and (HS)CS fragment whereas pathway 2 involve acidic H-abstraction which results into single-water molecule and S(HC)S fragment. As depicted in Figures 1 and 3, pre-reaction complex B2 along path II is lower-lying and hence is more stable than complex B1 along path I. Moreover, the relative energy of transition state TS2 along path II is lower than TS1 along path I. TS2 involves the interactions of acidic H-atom (on sulfur) with the O-atom of the oxidizing OH radical at a distance of 1.352 Å with elongation of the S–H bond to 1.443 Å, as observed at the BHandHLYP/6-311++G(d,p) level of the theory. It should be noted that the product-structures formed, P1 along formyl hydrogen abstraction pathway is more stable while P2 along acidic hydrogen abstraction pathway is less stable than the separated products. As evident in Figure 3, and from the standard Gibbs free-energy change listed in Table 2, the acidic H-abstraction is found to be thermodynamically and kinetically more favorable than the formyl H-abstraction. Though, similar formyl H-abstraction reaction pathways were also observed for thiol-form of thioformic acid (TFA) in our previous study,[4] but the acidic H-abstraction was observed to be only thermodynamically favorable.

It is worth-noting that OH radical in TS1 is oriented in the HCS plane of DTFA in such a manner that its unpaired electron interacts with H1-atom to be abstracted, thereby, forming a 3 centre-3 electron bond which causes triplet repulsions between the unpaired electron located at C1 and O1 atom involved in the hydrogen abstraction corresponding to a free-radical mechanism. Moreover, NBO spin density analysis of TS1 as listed in Table 3 shows that the (spin density) is concentrated on C1(0.198) and O1(0.683) with small negative value on H1(-0.057) atom. However in TS2, though the orientation of OH radical is also in

the HSCS plane of DTFA but instead of following the conventional free-radical mechanism, it may follow PCET mechanism. Through the latter, the lone pair of OH radical interacts with hydrogen atom (H3) to be abstracted whereas its unpaired electron interact with the lone pair of sulfur (S2) atom in DTFA. An investigation of the MOs of TS2 suggests that there may be a concerted movement of electron (from the sulfur atom, in DTFA, to the oxygen atom of the OH radical), and proton being abstracted from the DTFA, as evident in Figure 4a depicting a probable PCET in the highest singly occupied β MO. This is further supported by the (spin density) analysis of TS2 in Table 3 which shows that the spin density is concentrated on O1(0.168) and S2(0.840) whereas on S1(0.001) it is negligible. However, it should be noted that water-free oxidation could not be traced at the MP2 and other DFT methods employing B3LYP, and ω-B97XD functionals applied in the present work, except path II which was successfully traced using DFT/M06-HF besides DFT/BHandHLYP.

Water-Catalyzed Oxidation Pathways

As depicted in Figure 2, most of the ternary pre-reaction complexes, obtained by ADDF search, exhibit a significant interaction of DTFA with water, which can be formed by interaction of the oxidizing OH radical with the binary complex of DTFA with H_2O such as B3, B4, B5 and B6. The ternary pre-reaction complexes, C5 and C6, seem to be formed by interaction of HSCSH-OH (complex B2 in Figure 1) with the stabilizing H_2O since water is coordinating only with the OH radical. The binary complexes of DTFA with water observed were found to be less stable while those with hydroxyl radical were found to be more stable than the sum of separated reactants by 9.85-10.10 kcal/mol and 1.26-2.26 kcal/mol, respectively, at the CCSD(T)/6-311++G(d,p)//BHandHLYP/6-311++G(d,p) level of the theory. As depicted in Figures 2 and 3, pre-reaction binary complexes B3 and B4 along path III and IV, respectively, involving the formyl H-abstraction, and complexes B5 and B6 along path V and VI, respectively, involving the acidic H-abstraction possesses the same geometry

and energy. Noticeably, B4 or B6 lie lower in energy than B3 or B5 due to the presence of six-membered ring association between DTFA and water molecule, while B3 or B5 forms a five-membered ring association leading to higher ring strain. These binary complexes further react with the OH radical to form ternary pre-reaction complexes C1-C6 depicted in Figure 2. The products formed along water-catalysed formyl hydrogen abstraction pathways are more stabilized while those along acidic hydrogen abstraction pathways are less stabilized than the separated reactants as in case of water-free pathways. As evident in Figure 2a, the stabilization effect of water is observed to be more in the complex C1 along path III than that in the complex C2 along path IV because water directly interacts with OH in C1, whereas water lies on different side of DTFA in C2. Though the governing transition state, TS3 along path III, for formyl-hydrogen abstraction lays lower than TS4 along path IV for the same H-abstraction but the reaction barrier along path III is 8.28 kcal/mol while along path IV, it is 6.15 kcal/mol as evident in Figure 3. These pathways finally leads to the formation of two water molecules and (HS)CS fragment. Both of these water catalyzed formyl-hydrogen abstraction pathways were also traced for TFA(thiol) in our previous study,[4] and reaction pathway similar to path III was found to be kinetically more feasible, and follows radical mechanism as evident from Table 3.

In the case of water catalysed acidic hydrogen abstraction pathways V and VI depicted in Figure 2b, water stabilization is found to be more in ternary complex C4 than C3 due to the same reason as observed for C1 and C2 along the formyl hydrogen abstraction pathways. It is worth noting that once C3 is formed along path V, it immediately releases heat and result into two water molecules and S(HC)S fragment since the reaction barrier and ΔG to reach lowest-lying TS5 is respectively, -1.45 and -0.56 kcal/mol as depicted in Table 1 and 2. However, path VI for the water-catalysed acidic hydrogen abstraction shows the negative catalytic effect since TS6 lays 22.53 kcal/mol higher in energy than the TS1, and the

transition barrier is 34.08 kcal/mol. The computations show that the acidic H-abstraction pathway along path V is more feasible since it follow exothermic route, as evident in Figure 3 and Table 2. As shown in Figure 3, B2 complex observed along water-free pathway II is most stable among all the binary complexes which can further react with a water molecule to form two ternary pre-reaction complexes C5 and C6 along path VII and VIII depicted in Figure 2c, finally leading to the acidic hydrogen abstraction resulting in two water molecules and S(HC)S fragment. These two pathways (VII and VIII) were not observed in our previous study on TFA.[4] As seen in Figure 3, ternary complexes C5 and C6 are the most stable complexes among all the pre-reaction complexes. Though the geometries of C5 and C6 are similar but they differ in the orientation of coordinated water. In C5, water lies below the plane of DTFA while it lies above the DTFA plane in C6.

Interestingly, the relative energy of the transition state TS7 along the acidic hydrogen abstraction path VII is the second lowest lying while TS8 along path VIII is the second highest lying (showing negative catalysis) among all the located TSs along the water-catalyzed and water-free pathways. Notably, the geometry of TS7 involves a five-membered ring formation between the DTFA and the O-atom of OH radical which further interacts with the water molecule. The investigation of occupied MOs and (spin density) distribution from NBO analysis of TS7, as depicted in Table 3, demonstrate that the PCET mechanism may operate along path VII, since an unpaired electron in TS7 is found to be shared by the O-atom(0.434) of the oxidizing OH lying orthogonal to the HSCS plane of DTFA and thiocarbonyl S-atom (0.629) of DFTA. Moreover, all other water-catalysed acidic hydrogen abstraction pathways explored may follows PCET mechanism due to the same reason as explained for path II along the water-free pathway as depicted in Figure 4 and Table 3.

Comparing the water-free oxidation with the water-catalysed oxidation of DTFA by hydroxyl radical presented in this work, the catalytic pathway is observed to be more feasible

except path VI and VIII. Most of the catalytic TSs are low lying in energy than the non-catalytic TSs as indicated in Figure 3. For instance, the relative energy of TS2 along the water-free pathway is 7.53 kcal/mol more than TS5 along the water-catalyzed pathway. Moreover, as evident from Table 2, the ΔG to reach the transition state TS2 along the water-free pathway is relatively higher than that required for TS5 along the water-catalyzed pathway. The products, (HS)CS and S(CH)S, formed in the water-catalyzed formyl and acidic hydrogen abstraction pathways are more stabilized than those in the water-free formyl and acidic hydrogen pathways, respectively, due to the stabilization caused by water molecule forming the hydrogen bonds.

For further analysis, computations of the reaction species were also performed at the CCSD(T)/6-311++G(2d,2p)//MP2/6-311++G(2d,2p) level of theory. However, at this level of the theory, pre-reaction complexes B2, C5, C6 and transition states TS1, TS2, TS5-TS8 failed to optimize. In fact, at this level of the MP2 theory, pathways for only formyl-hydrogen abstraction catalyzed by water could be traced. In particular, path III was found to be both kinetically and thermodynamically most feasible at CCSD(T)/6-311++G(2d,2p)//MP2/6-311++G(2d,2p) level of theory. It seems that the inter-electron correlations among fragments in the transition states and pre-complexes are significantly affecting the reaction pathways. In order to check the validity of the pathways traced at the level of DFT/BHandHLYP/6-311++G(d,p), further computations were carried out at hybrid B3LYP/6-311++G(d,p) and dispersion-corrected ω-B97XD/6-311++G(d,p) levels of the DFT. However, only pathways III, IV and VI could be confirmed at these DFT levels. Notably, computations with self-interaction free DFT/M06-HF/6-311++G(d,p) revealed all the pathways except I and VI. Only pathways III and IV could be traced by all the different theoretical methods applied in this work. The energies of the species along the most feasible pathways III and IV explored are further compared at BHandHLYP and M06-HF levels of theory to analyse the self-

interaction correction as listed in Table 5. It was noticed that when the self-interaction correction in the energy is accounted for as using DFT/M06-HF method, then the path III is observed to be exothermic contrary to that using the DFT/BHandHLYP method. However, there is little impact on Path IV due to this.

To further enquire into the stability of reaction complexes with respect to respective dissociation fragments, standard Gibbs free energy change at different temperature was analyzed as provided in Table 4. The complexation of DTFA with OH radical and H_2O molecule is found to increase with the decrease in temperature as evident from the increasingly positive free energy change with decrease in the temperature for the dissociation reaction of the complexes. Interestingly, all the binary and ternary complexes seem to be more stable at lower temperature particularly below 150 K. It should be noted that the ternary complexes are more stabilized than the binary complexes at lower temperatures due to presence of more number of hydrogen-bond with the addition of a water molecule.

Conclusion

The reaction pathways explored in this work are able to successfully exhibit the catalytic effect of water on the gas phase oxidation of DTFA by hydroxyl radical, however, this could not be revealed by all the different theoretical methods employed for their investigation. Interestingly, the coordinated water molecule in the pre-reaction complexes, was observed to be not directly involved in the hydrogen abstraction process, rather it lowered the reaction barriers through the hydrogen bonds. The acidic hydrogen abstraction in DTFA was found to be thermodynamically as well as kinetically feasible in both catalytic and non-catalytic processes. The most feasible pathway involving catalytic acidic hydrogen abstraction was found to be exothermic and follows a PCET mechanism rather than a free-radical mechanism observed in the formyl-hydrogen abstraction pathways. However, only

catalytic formyl-hydrogen abstraction could be revealed at all the different theoretical methods applied. Besides these, the formation of reaction complexes is observed to be more feasible than their dissociation at temperatures below 150 K.

Finally, as also emphasized in the introductory section, the reaction pathways traced by the IRCs and ADDs need not to be always followed by the actual atomic-level dynamics, and there may be several non-IRC pathways available.[20] For example, non-IRC dynamics for the proton transfer had been reported in the literature.[23-24] For a three-body system like the water-catalyzed reaction investigated in the present work, performing a molecular dynamics simulation is a complex task though quite interesting and challenging.

Acknowledgements

One of the authors, GK, thanks University Grants Commission (UGC), India for providing financial support in the form of UGC-SRF(NET) fellowship. The authors are also grateful to Prof. Koichi Ohno for providing GRRM program, and to Dr. Neetu Goel and the Department of Chemistry, Panjab University, Chandigarh, for providing other computational software and resources.

References

1 E. Vohringer-Martinez, B. Hansmann, H. Hernandez, J. S. Francisco, J. Troe, B. Abel, *Science*, 2007, **315**, 497−501.

2 C. Iuga, J. R. Alvarez-Idaboy, A. Vivier-Bunge, *Chem. Phys. Lett*., 2010, **501**, 11−15.

3 Y. Luo, S. Maeda, K. Ohno, *Chem. Phys. Lett*., 2009, **469**, 57−61.

4 G. Kaur, Vikas, *J. Phys. Chem. A,* 2014, **118**, 4019-4029.

5 G. Kaur, Vikas, Phys. Chem. Chem. Phys., 2014, **16**, 24401-24416.

6 K. Ohno, S. Maeda, *Chem. Phys. Lett.,* 2004, **384**, 277-282.

7 S. Maeda, K. Ohno, *J. Phys. Chem. A,* 2006, **110**, 8933-8941.

8 S. Maeda, K. Ohno, *J. Phys. Chem. A,* 2005, **109**, 5742-5753.

9 S. Maeda, K. Ohno, *Chem. Phys. Lett.,* 2005, **404**, 95-99.

10 S. Maeda, K. Ohno, K. Morokuma, *Phys. Chem. Chem. Phys*., 2013, **15**, 3683-3701.

11 S. Maeda, Y. Osada, K. Morokuma, K. Ohno, GRRM 11 user manual, 2011(http://grrm.chem.tohoku.ac.jp/GRRM/).

12 C. Gonzalez, H. B. Schlegel, *J. Chem. Phys.,* 1989, **90**, 2154-2161.

13 C. Gonzalez, H. B. Schlegel, *J. Chem. Phys*., 1990, **94**, 5523-5527.

14 G. Kaur, Vikas, *Tetrahedron Lett*., 2015, **56**, 142–145.

15 R. Kaur, Vikas, *J. Chem. Phys*., 2015, **142**, 074307.

16 Vikas, G. Kaur, *J. Chem. Phys*., 2013, **139**, 224311-13 (Erratum: *J. Chem. Phys.* 2014, **141**, 039901).

17 G. Kaur, Vikas, *J. Comp. Chem.,* 2014, **35**, 1568-1576.

18 S. R. V. Linde, W. L. Hase, *J. Am. Chem. Soc.,* 1989, **111**, 2349-2350.

19 J. Zhang, U. Lourderaj, R. Sun, J. Mikosch, R. Wester, W. L. Hase, J. Chem. Phys., 2013, **138**, 114309-114322.

20 J. G. Lopez, G. Vayner, U. Lourderaj, S. V. Addepalli, S. Kato, W. A. deJong, T. L. Windus, W. L. Hase, *J. Am. Chem. Soc.,* 2007, **129**, 9976-9985.

21 J. Xie, R. Sun, M. R. Siebert, R. Otto, R. Wester, W. L. Hase, *J. Phys. Chem. A*, 2013, **117**, 7162−7178.

22 L. Sun, K. Song, W. L. Hase, *Science*, 2002, **296**, 875-878.

23 P. L. Houston, S. H. Kable, *Proc. Natl. Acad. Sci. U.S.A.,* 2006, **103**, 16079-16082.

24 M. A. ter Horst, G. C. Schatz, L. B. Harding, *J. Chem. Phys.,* 1996, **105**, 558-571.

25 T. Rog, K. Murzyn, J. Milhaud, M. Karttunen, M. Pasenkiewicz-Gierula, *J. Phys. Chem. B*, 2009, **113**, 2378-2387.

26 A. C. Storer, W. F. Murthy, P. R. Carey, *J. Biol. Chem.,* 1979, **254**, 3163-5.

27 G. Lowe, A. Williams, *J. Biochem.,* 1965, **96**, 189-193.

28 J. J. C. Teixeira-Dias, V. M. Jardim-Barrreto, Y. Ozaki, A. C. Storer, P. R. Carey, *Can. J. Chem.,* 1982, **60**, 174.

29 A. D. Becke, *J. Chem. Phys.,* 1993, **98**, 1372-77.

30 K. Raghavachari, G. W. Trucks, J. A. Pople, M. Head-Gordon, *Chem. Phys. Lett*., 1989, **157**, 479-483.

31 S. F. Boys, F. Bernardi, *Mol. Phys.*, 1970, **19**, 553-566.

32 M. Head-Gordon, J. A. Pople, M. J. Frisch, *Chem. Phys. Lett.,*1988, **153**, 503-506.

33 K. Kim, K. D. Jordan, *J. Phys. Chem. A*, 1994, **98**, 10089–10094.

34 D. Chai, M. Head-Gordon, *Phys. Chem. Chem. Phys.*, 2008, **10**, 6615-20.

35 Y. Zhao, D. G. Truhlar, *J. Phys. Chem. A Lett.,* 2006, **110***,* 13126-13130.

36 M. J. Frisch, G. W. Trucks, H. B. Schlegel, G. E. Scuseria, M. A. Robb, J. R. Cheeseman, Jr. J. A. Montgomery, T. Vreven, K. N. Kudin, J. C. Burant, et al. Gaussian 03, revision E.01; Gaussian, Inc.: Wallingford, CT, 2004.

37 Frisch, M. J.; Trucks, G. W.; Schlegel, H. B.; Scuseria, G. E.; Robb, M. A.; Cheeseman, J. R.; Scalmani, G.; Barone, V.; Mennucci, B.; Petersson, G. A. et al. Gaussian 09 Revision D.01; Gaussian, Inc., Wallingford CT, 2013.

38 T. J. Lee, P. R. Taylor, *Int. J. Quantum Chem*., 1989, **S23**, 199-207.

39 S. P. So, *J. Mol. Struct. Theochem.,* 1986, **148**, 153-161.

40 M. H. V. Huynh, T. J. Meyer, *Chem. Rev.,* 2007, **107**, 5004–5064.

41 F. Weinhold, *J. Comput. Chem.,* 2012, **33**, 2363–2379.